Inverse Problems, Design and Optimization Symposium
Rio de Janeiro, Brazil, 2004

CONSTRUCTAL OPTIMIZATION COMBINING HEAT TRANSFER WITH OTHER DISCIPLINES

Louis Gosselin[1, 2] *Louis.Gosselin@gmc.ulaval.ca*
Adrian Bejan[2] *dalford@duke.edu*
Sylvie Lorente[3] *lorente@insatlse.insa-tlse.fr*

[1]Département de génie mécanique
Université Laval
Québec, Québec, CANADA

[2]Department of Mechanical Engineering and Materials Science, Duke University
Durham, North Carolina, USA

[3]Département de Génie Givil et Urbanisme
Institut national des sciences appliquées
Toulouse, FRANCE

ABSTRACT

This paper outlines recent work on the extension of constructal design to multi-objective systems. The optimization of two types of systems is investigated. The first system is an electromagnet in which hot spot temperature must be minimized, and magnetic performance maximized. The second type of systems consists of beams, that must provide at the same time great strength, and large time of survival in case of thermal attacks. In both cases, volume constraint is invoked. We show how shape and structure are generated by the competition that takes place between the various objectives and constraints during the geometric optimization process.

NOMENCLATURE

B_0	magnetic induction at the center of the coil, T
D	half-thickness of a cooling disc, m
E	elastic modulus, Pa
G	dimensionless magnetic parameter
H	beam profile, m
j	current density, A m^{-2}
k	thermal conductivity, W m^{-1} K^{-1}
L	length, m
m	shape parameter
M	moment, N m
n	number of cooling discs
P	total power dissipated, W
q"	heat flux, W m^{-2}
q"'	volumetric heat source, W m^{-3}
$\tilde{q}$	dimensionless volumetric heat source
r	radial position, m
r_0	inner radius, m
r_1	outer radius, m
t	time, s
T	temperature, K
T_0	sink temperature, K
V	solenoid volume, m^3
x, y	Cartesian coordinates, m
Z	thickness of elastic core, m

Greek Symbols

β	coefficient characterizing yield stress temperature dependence, K^{-1}
δ	beam deflection, m
θ	dimensionless temperature
ϕ	fraction of the volume occupied by the discs
ρ	electrical resistivity, W m A^{-2}
σ	stress, N m^{-2}

Subscripts

y	yield point

Superscripts

~	dimensionless variables

1. INTRODUCTION

Imagining better and better designs has always been a central goal of engineering. The first conceptual step of this process is to recognize what "better" means. This step consists of identifying the objective, which is to maximize global performance, while acknowledging the global constraints. This step must be made early in the designing process, *before* the system takes shape. The geometry is the unknown. In the pursuit of better global performance under

constraints, more efficient configurations are generated. The view that geometry is generated by the pursuit of global performance under global constraints has been named constructal theory [1].

In earlier works, shape and structure were generated by addressing only one objective. However, even the simplest systems usually have more than one objective. This calls for extending the constructal approach to multi-objective systems. In this paper, we outline two problems to illustrate how this can be realized.

The first system is an electromagnet. Cooling must be provided to the magnet for managing heat generation, and at the same time, the designer faces magnetic performance requirement and volume constraint. Beams are the second type of systems that we consider. As a mechanical structure, a beam must have a small deflection in the absence and presence of a thermal attack. For both problems, we show how the optimal geometry emerges from the competition between the various objectives.

2. OPTIMIZATION OF AN ELECTRO-MAGNET

Figure 1 shows the front and side view of a solenoid [4-7]. It consists of several layers of wire wound around a cylinder of radius r_0. The coil outer radius and length are respectively r_1 and 2L. When a current passes through the wire, it generates a one-dimensional magnetic field on the coil centerline. However, because of the Joule effect, the current also generates heat, leading to a temperature rise. For preserving the coil integrity, one should minimize the magnet temperature. Furthermore, electrical resistivity of coil materials usually increases with temperature, leading to a more expensive to operate device. In this section, we consider both requirements: intense magnetic field, and low temperatures.

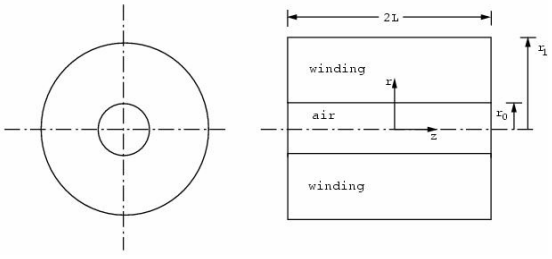

Figure 1: Electromagnet geometric features.

2.1. Magnetic Point of View

Consider a uniform current density j that flows in the winding. The magnetic field is maximum at the origin (z = r = 0), and at that position is given by [2-3]:

$$B_0 = 0.2\pi j \int_{-L/2}^{L/2} \left(\int_{r_0}^{r_1} \frac{r^2\, dr}{\left(r^2 + z^2\right)^{3/2}} \right) dz \qquad (1)$$

The total power dissipated in the coil can be calculated by

$$P = 2\pi\rho j^2 \int_{-L/2}^{L/2} dz \int_{r_0}^{r_1} r\, dr \qquad (2)$$

Combining Eqs. (1) and (2), it is possible to write the magnetic field at the origin as:

$$B_0 = \left(\frac{P}{\rho r_0}\right)^{1/2} G\left(\frac{r_1}{r_0}, \frac{L}{r_0}\right) \qquad (3)$$

The first term on the right-hand side of (3) is a constant. The dimensionless function G depends only on the coil geometry,

$$G = 0.2 \left(\frac{2\pi\tilde{L}}{\tilde{r}_1^2 - 1}\right)^{1/2} \ln \frac{\tilde{r}_1 + \left(\tilde{L}^2 + \tilde{r}_1^2\right)^{1/2}}{1 + \left(\tilde{L}^2 + 1\right)^{1/2}} \qquad (4)$$

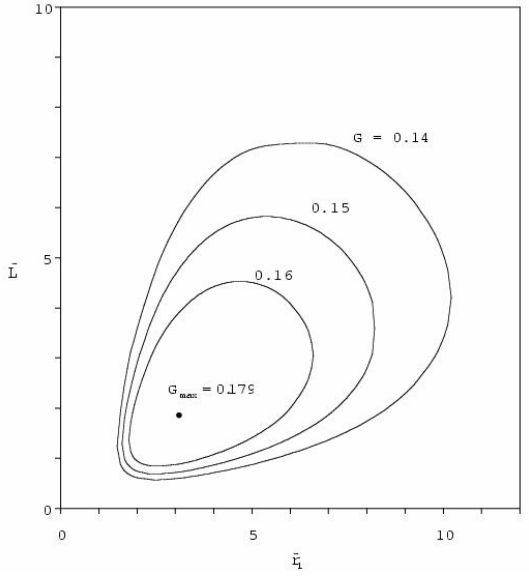

Figure 2: Parameter G in the $\tilde{r}_1 - \tilde{L}$ plane.

where the coil inner radius r_0 has been used to non-dimensionalized the magnet dimensions (r_0 is typically determined by the application where the magnet is used),

$$\left(\tilde{r}_1,\ \tilde{L}\right) = \frac{(r_1,\ L)}{r_0} \tag{5}$$

Eq. (4) is reported graphically in Fig. 2. All the points on a constant-G line have the same magnetic performance. In other words, for a given power P, all the designs represented by a constant-G line lead to the same magnetic field. The question is now which one leads to the smallest hot spot temperature, i.e. to the best thermal performance.

2.2. Thermal Point of View

Different cooling systems can be considered. Here we study the insertion of n high thermal conductivity discs of thickness 2D in contact with a cold reservoir at a temperature T_0, Fig. 3. The conductivity of the discs, k_1, is assumed much larger than the one of the winding, k_0, hence $\tilde{k} = k_1/k_0 >> 1$. The function of the discs is simply to extract the heat generated in the coil and to lead it to the cold reservoir. The fraction of the volume occupied by the discs is assumed to be fixed,

$$\phi = \frac{Dn}{L} \tag{6}$$

For compactness reason, we have $\phi << 1$. This also ensures that the presence of the inserts does not modify greatly the magnetic field, i.e. that Eq. (4) is valid. The temperature profile can be estimated analytically or numerically by solving the conduction equation,

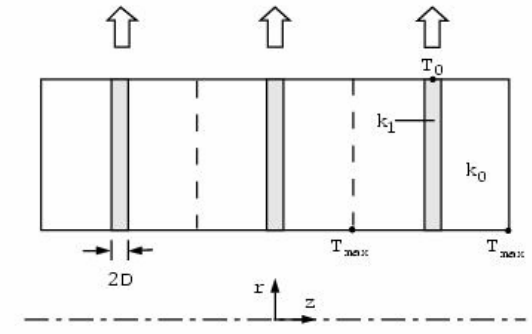

Figure 3: Geometry of the cooling system.

$$\frac{1}{\tilde{r}}\frac{\partial}{\partial\tilde{r}}\left(\tilde{r}\,\frac{\partial\theta}{\partial\tilde{r}}\right) + \frac{\partial^2\theta}{\partial\tilde{z}^2} + \frac{\tilde{q}}{\tilde{k}} = 0 \tag{7}$$

where:

$$\theta = \frac{T - T_0}{P/(r_0 k_0)},\ \tilde{q} = \frac{1}{\tilde{V}},\ \tilde{V} = \pi\tilde{L}\left(\tilde{r}_1^2 - 1\right) \tag{8}$$

For example, based on the arguments that $k_1/k_0 >> 1$ and $\phi << 1$, it can be shown analytically [14] that the hot spot temperature is given by:

$$\theta_{max} = \frac{\tilde{L}}{2\pi n^2\left(\tilde{r}_1^2 - 1\right)} + \frac{1}{2\pi\phi\tilde{k}\tilde{L}}\left(\frac{1}{2} - \frac{\ln\tilde{r}_1}{\tilde{r}_1^2 - 1}\right) \tag{9}$$

2.3. Combining Heat Transfer and Magnetism

For all the designs with a given magnetic performance, i.e. all the points on a constant-G curve, we calculated the hot spot temperature either with analytical formula, Eq. (8), or with a finite element code [8]. We repeated this procedure for different values of n, the number of cooling discs. In these calculations, ϕ was kept constant. The optimal results are presented in Fig. 4 for different number of discs. The hot spot temperature decreases as the number of discs increases. The downside of this is that a more complex solenoid would have to be built.

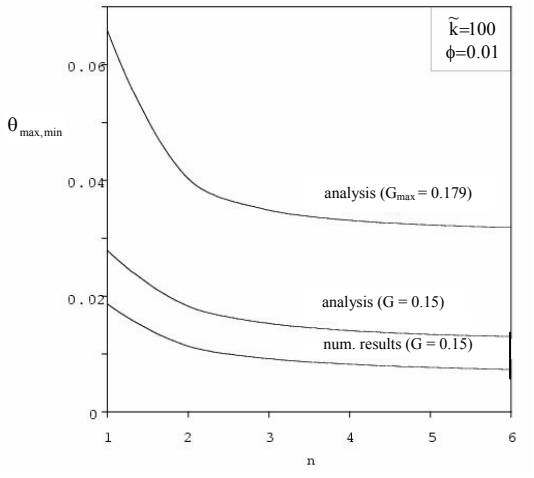

Figure 4: Minimum hot spot temperature as a function of the number of cooling discs.

A more refined approach consists of relaxing the assumption that $\phi << 1$. An equivalent G-parameter that takes into account the presence of the discs can be used, because in fact, the discs do not contribute to the magnetic field generation. There is a clear tradeoff: when ϕ is too small, the coil is not cooled properly, when ϕ is too large, it is hard to reach large magnetic field. The optimal is in-between. For example, for n = 1, the equivalent G that takes into account the presence of the inserts is,

$$G_{eq,n=1} = \frac{G_{\tilde{L}}\tilde{L}^{1/2} - G_{\tilde{D}}\tilde{D}^{1/2}}{\left(\tilde{L} - \tilde{D}\right)^{1/2}} \qquad (10)$$

where:

$$G_{\tilde{L}} = 0.2\left(\frac{2\pi\tilde{L}}{\tilde{r}_1^2 - 1}\right)^{1/2} \ln\frac{\tilde{r}_1 + \left(\tilde{L}^2 + \tilde{r}_1^2\right)^{1/2}}{1 + \left(\tilde{L}^2 + 1\right)^{1/2}} \qquad (11)$$

$$G_{\tilde{D}} = 0.2\left(\frac{2\pi\tilde{D}}{\tilde{r}_1^2 - 1}\right)^{1/2} \ln\frac{\tilde{r}_1 + \left(\tilde{D}^2 + \tilde{r}_1^2\right)^{1/2}}{1 + \left(\tilde{D}^2 + 1\right)^{1/2}} \qquad (12)$$

Another step is to constrain coil volume, for the sake of compactness. It is worth noting that $\tilde{L}$ and $\tilde{D}$ are now independent variables, because the percentage of the volume occupied by the disc (ϕ) is not fixed, but must be optimized. The external shape features ($\tilde{L}$, $\tilde{r}_1$) are linked via the total volume constraint, Eq. (8). Fixing $G_{eq,n=1}$, P and $\tilde{V}$ leaves only one degree of freedom. We choose $\tilde{L}$ as this degree of freedom.

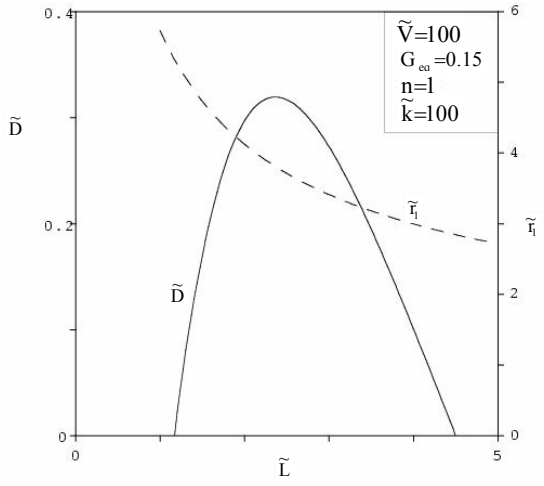

Figure 5: D and r_1 as a function of L.

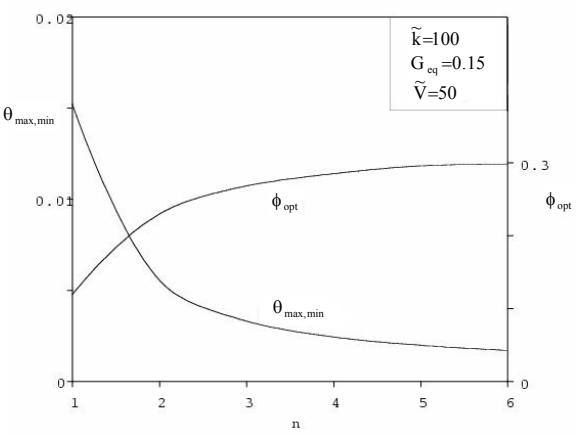

Figure 6: Constrained $\tilde{V}$ and G_{eq} optimal results.

Figure 5 shows how $\tilde{D}$ and $\tilde{r}_1$ vary with $\tilde{L}$. All the designs of Fig. 5 are equivalent magnetically ($G_{eq,n=1}$ = 0.15) and have the same mass or volume ($\tilde{V}$ = 100). We want to find out which of these designs performs best from the thermal point of view. To this end, we vary $\tilde{L}$, and solve Eq. (7) numerically. The procedure is repeated for different values of n. The results are presented in Fig. 6. As n increases the hot spot temperature first drops dramatically, and then continues to decrease slowly. The optimal ratio of the volume occupied by the high thermal conductivity material is also plotted in Fig. 6.

3. OPTIMIZATION OF A BEAM TO FACE THERMAL ATTACK

In this section, we combine heat transfer and structural analysis with the help of the constructal method: we study systems that must be mechanically strong and, at the same time, must retain their strength and integrity during thermal attack. Mechanical structures become weaker and may collapse if they are exposed to intense heating [13, 15].

The classical approach to providing a structure with thermal resistance against intense heating is by coating the structure with a protective layer *after* the structure has been designed. Here, we propose to change the conceptual approach to optimal structures, away from the single-objective lessons of the past, and in line with the two-objective morphing of structures shown in Ref. [9]. We illustrate this approach by optimizing beams in pure bending exposed to sudden heating. The solid structure is penetrated by time-dependent conduction heating. We show that the

mechanical and thermal objectives compete, and that this competition generates the optimal geometry of the system.

3.1. Stiffness Point of View

Consider a beam simply supported at each end, Fig. 7. The beam geometry is two-dimensional, with the length L and symmetric profile H(x). The total load F [N/m] is distributed uniformly over the beam length L. The force F is expressed per unit length in the direction perpendicular to the plane of Fig. 7. The weight of the beam is assumed to be negligible in comparison with the load. The beam profile is sufficiently slender so that its deformation in the y direction is due mainly to pure bending.

The beam is initially isothermal at the ambient temperature T_∞, where it behaves elastically throughout its volume. The modulus of elasticity is E, which for simplicity is assumed constant. Thermal attack means that at the time t = 0 the beam is exposed on both surfaces to the uniform heat flux q". Temperatures rise throughout, but they rise faster in the subskin regions, Fig. 8. These are the first regions where the material behavior changes from elastic to plastic. The last to undergo this change is the core region of thickness Z(x), in which the material behaves elastically.

The total bending moment in a constant-x cross-section is (e.g., Refs. [10-11])

$$\frac{M}{W} = \frac{FL}{2}\frac{x}{L}\left(1-\frac{x}{L}\right) \qquad (13)$$

where W is the beam length in the z direction, which is perpendicular to the plane of Fig. 7. This moment is balanced by the moment due to the tensile and compressive stresses (σ) that are present in the cross-section. When σ is less than the yield stress σ_y, the material behaves elastically. The yield stress decreases as the local temperature increases. For simplicity, we assume a linear model for the effect of T on σ_y,

$$\frac{\sigma_y}{\sigma_{y,ref}} = 1 - \beta\,(T - T_{ref}) \qquad (14)$$

where the β coefficient is a property of the material, and T_{ref} is a reference temperature, such that $\sigma_{y,ref} = \sigma_y(T_{ref})$. It is convenient to set the reference temperature to the ambient temperature, $T_{ref} = T_\infty$ and $\sigma_{y,ref} = \sigma_{y,\infty}$. In the elastic core the stresses vary linearly (e.g., Ref. [10-11]),

$$\frac{\sigma}{\sigma_y} = \frac{y}{Z/2} \qquad (15)$$

In this expression σ_y is the yield stress at $y = \pm Z/2$, which is associated with the instantaneous temperature at that location. We assume that in the peripheral regions outside $y = \pm Z/2$ the material is perfectly plastic, so that σ is equal to $\sigma_y(T)$, where T is the local temperature.

Figure 8 summarizes qualitatively the distribution of stresses in the cross-section, at a time when plastic regions are present, Z < H. In this model we accounted for the fact that in the beginning there is a time interval when the entire beam is elastic, and the maximum stress (σ_{max}, at $y = \pm H/2$) is still below the yield stress. During this initial time interval the beam deflection is constant in time. The moment formed by the stresses in the beam cross-section,

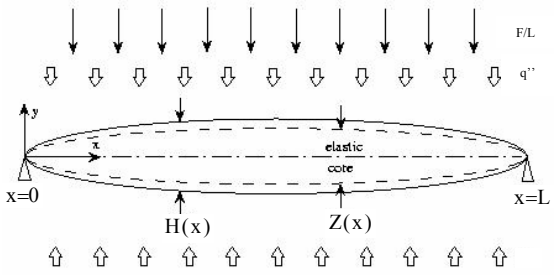

Figure 7: Beam geometry.

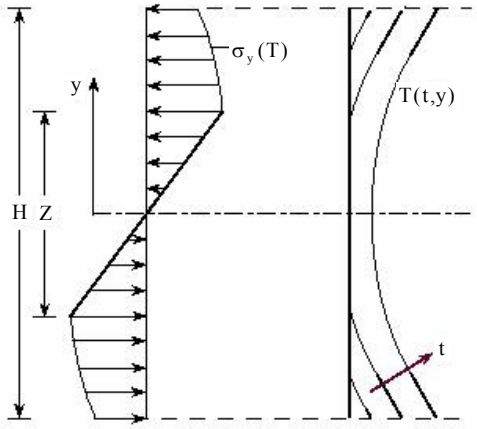

Figure 8: Stress distribution in the beam.

$$\frac{M(x,t)}{W} = \int_{-H/2}^{H/2} \sigma(t,x,y)\, y\, dy \qquad (16)$$

leads to a two-term expression that accounts for the elastic and plastic regions,

$$\frac{M}{W} = \frac{1}{6}\sigma_y\left[T(t,x,y=Z/2)\right]Z^2 + 2\sigma_{y,ref}\int_{Z/2}^{H/2}(1-\beta\Delta T)\, y\, dy \qquad (17)$$

where

$$\sigma_y\left[T(t,x,y=Z/2)\right]=\sigma_{y,ref}[1-\beta\Delta T(t,x,y=Z/2)] \qquad (18)$$

$$\Delta T(t, x, y) = T(t, x, y) - T_\infty \qquad (19)$$

Equations (12) and (16) can be combined to pinpoint the location of the elastic-plastic interface, Z(t, x), for a specified beam profile H(x), and temperature distribution T(t, x, y).

Consider next the beam deflection in the y direction. The local radius of curvature ρ of the deformed beam is (e.g., Refs. [10-11]),

$$\rho(t,x) = \frac{EZ(t,x)}{2\sigma_{max}} \qquad (20)$$

As a first approximation, for small deflections the position of the neutral line [y = δ(x)] can be written as

$$\frac{d^2\delta}{dx^2} = \frac{1}{\rho} \qquad (21)$$

In the absence of a plastic zone, the stress in the outer fibers (y = ± H/2) is

$$\sigma_{max} = \frac{3F}{H^2}\, x\left(1-\frac{x}{L}\right) \qquad (22)$$

which must be used in Eq. (20). On the other hand, when a plastic zone is present, the maximum stress is reached at the plastic-elastic interface, $\sigma_{max} = \sigma_y\,[T(Z/2)]$. Equation (21) can be integrated twice to obtain the position of the neutral line. The boundary conditions are

$$\delta = 0 \quad \text{at} \quad x = 0 \quad \text{and} \quad x = L \qquad (23)$$

The maximal deflection occurs in the midplane,

$$\delta_m = -\,\delta(x = L/2) \qquad (24)$$

The amount of beam material is fixed, and, in view of the two-dimensional geometry of Fig. 7, the profile area is also fixed,

$$A = \int_0^L H(x)\, dx \qquad (25)$$

We considered many profile shapes, e.g., Eq. (28) in the next section. For every assumed shape, we calculated numerically the time evolution of the maximal deflection, $\delta_m(t)$. The objective is to identify the shape for which δ_m is the smallest at a given t. This shape is the most resistant to thermal attack.

3.2. Heat Transfer Point of View

The local beam temperature is known from Fourier analysis [12], under the assumption that the beam profile is slender so that conduction in the x direction is negligible:

$$\Delta\tilde{T} = \tilde{H}\left[\tilde{t} + \frac{\tilde{y}^2}{6} - \frac{1}{6} - 2\sum_{n=1}^{\infty}\frac{(-1)^n}{n^2\pi^2}\, e^{-n^2\pi^2\tilde{t}}\cos(n\pi\tilde{y})\right] \qquad (26)$$

The dimensionless variables are defined in the next section. The infinite sum in the square brackets is important only in the beginning, and vanishes rapidly for $\tilde{t} > 1$.

3.3. Combining Heat Transfer and Stiffness Requirements for Optimal Beam Profiles

The numerical work was conducted in dimensionless terms by using the dimensionless variables:

$$\tilde{x} = \frac{x}{L} \qquad \tilde{y} = \frac{y}{H/2} \qquad \tilde{t} = \frac{\alpha t}{(H/2)^2}$$
$$\tilde{Z} = \frac{Z}{H} \qquad \tilde{H} = \frac{H}{L} \qquad \tilde{A} = \frac{A}{L^2}$$
$$\tilde{\beta} = \beta\,\frac{q''L}{2k} \qquad \tilde{\sigma} = \frac{\sigma}{F/L}$$
$$\tilde{\delta} = \frac{\delta E}{2F} \qquad \Delta\tilde{T} = \Delta T\,\frac{2k}{q''L} \qquad (27)$$

To start with, we considered a family of beam shapes that are smooth and thicker in the middle, e.g., Fig. 7:

$$\tilde{H} = C\left[\tilde{x}(1-\tilde{x})\right]^m \qquad (28)$$

The shape parameters C and m are related through the size constraint (26). The geometry is characterized by one shape parameter (m), which plays the role of degree of freedom, and by three construction parameters: $\tilde{A}$, $\tilde{\beta}$ and $\tilde{\sigma}_{y,ref}$. The calculation of $\tilde{\delta}_m(\tilde{t})$ is performed from $\tilde{t} = 0$ until the elastic core disappears at a location $\tilde{x}$. The model constructed in the preceding section is not valid when the elastic core is absent.

The numerical example given in Fig. 9 shows that the deflection increases in accelerated fashion in time, and that $\tilde{\delta}_m$ can be minimized by selecting the shape parameter m. This is the key result: the beam geometry can be selected in such a way that the beam as a whole is most resistant to thermal attack. This is a result for how the whole beam performs—a global result—because $\tilde{\delta}_m$ is a global feature. All the strained fibers contribute to $\tilde{\delta}_m$.

The influence of shape on performance is described further in Fig. 10, where $\tilde{\delta}_m(\tilde{t})$ has been plotted for three m values. Because the objective is to achieve the smallest $\tilde{\delta}_m$, we conclude that the best shape (m) changes as the time increases. The intersecting $\tilde{\delta}_m(\tilde{t})$ curves mean that m_{opt} decreases as $\tilde{t}$ increases. This decrease accelerates in time, as shown in Fig. 11. The same figure shows that the minimal mid-plane deflection $\tilde{\delta}_{m,min}$, which corresponds to the optimally changing shape $m_{opt}(\tilde{t})$, also accelerates in time. If $\tilde{t}$ denotes the prescribed life-time of the beam—the time in which it must withstand the thermal attack—then for every $\tilde{t}$ there exists an optimal beam shape.

Important in Figs. 10 and 11 are the short times, where deflections are small and comparable with deflections based on the assumption that thermal attack is absent. In this limit there is a definite beam shape that is optimal. This is also the limit in which the model constructed is valid.

4. CONCLUSIONS

Multi-objective systems are numerous and manifold, and to address simultaneously their objectives calls for truly interdisciplinary research. In this paper, we illustrated the interdisciplinary approach by showing that shapes and structures of beams can be optimized to face thermal attack, and that magnet can be optimized to perform efficiently from both the magnetic and thermal points of view. Examples of optimized shapes were the beam profile and cross-sectional aspect ratio, and the magnet length and outer radius. Optimized internal structure was the arrangement of the cooling discs in the magnets.

<

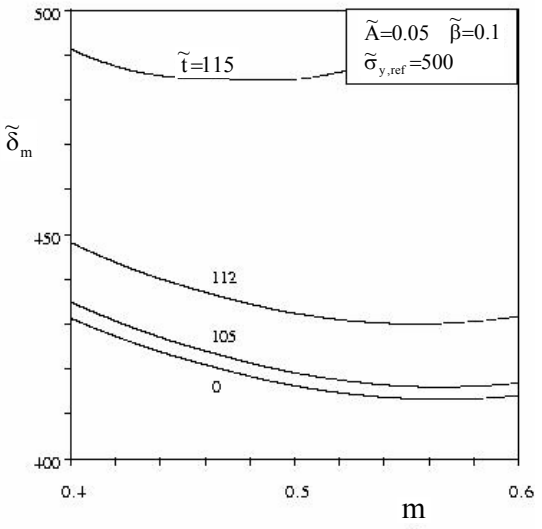

Figure 9: The existence of an optimal shape at each time.

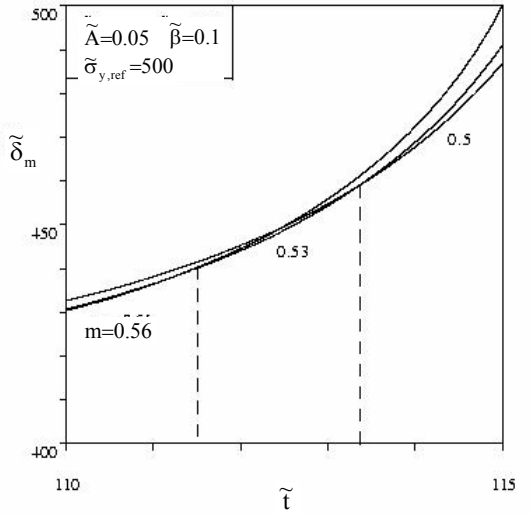

Figure 10: Time evolution of the optimal shape.

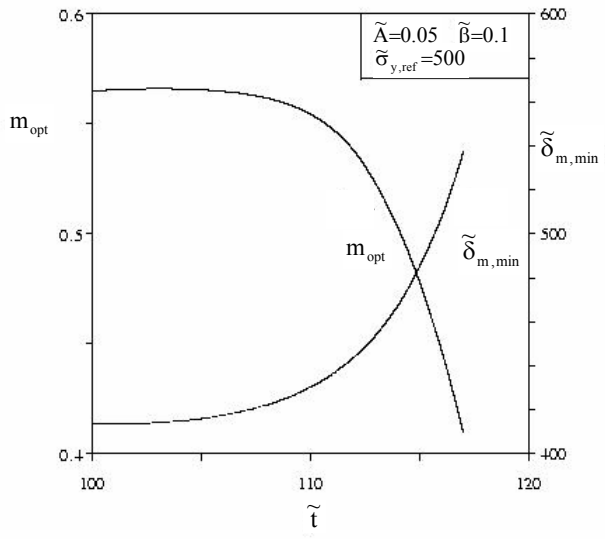

Figure 11: Influence of the shape on minimum deflection.

The optimal architecture of the multi-objective systems is a consequence of the competition between objectives. The work presented in this paper is fundamental and exploratory. More realistic models can be combined with the method outlined in this paper, in the pursuit of optimal architectures that serve more than one objective. Structures of greater complexity promise to benefit from the multidisciplinary approach advocated in this paper.

It is important not to confuse the method of constructal design with the blind optimization of every possible feature in a design that, if free, has an infinity of such features. We can consider design as flights of imagination. The difficulty is that flights of imagination translate into shorter and shorter leaps as structures become more complex. The challenge is to inspire flights of imagination early in the evolution of configuration, when the design is still nakedly simple. Problems such as the configurations of Figs. 3 and 7 are significant leaps forward from the amorphous black box with which an all-powerful code might start. To sense where the optimization opportunities lie requires intuition. One of the objectives of good research is to improve intuition. Constructal design efforts are oriented in that direction.

REFERENCES

[1] A. Bejan, *Shape and Structure, from Engineering to Nature*, Cambridge University Press, Cambridge, UK, 2000.

[2] Kroon, D. J., *Electromagnetics*, Philips Technical Library, Cambridge, MA, 1968.

[3] Montgomery, D. B., *Solenoid Magnet Design*, Wiley, New York, 1969.

[4] Herlach, F., Laboratory electromagnets—from oersted to megagauss, *Physica B* **319**, 321-329 (2002).

[5] Haignere, E. B. and Potter, W. M., Optimizing the shape and size of a uniform-current-density magnet to maximize the field at constant power, *J. Appl. Phys.* **47**, 1657-1661 (1976).

[6] Miklavc, A., The solenoid which gives the desired value of magnetic field for the smallest possible volume of conductor, *J. Appl. Phys*. **45**, 1680-1681 (1974).

[7] Morgan, P. N., Optimal design and construction of a lightweight minimum-power solenoid magnet, *IEEE Trans. Magn.* **37**, No. 5, September 2001.

[8] FIDAP Theory Manual, Fluid Dynamics International, Evanston, IL, Vol. 7.0, 1993.

[9] S. Lorente and A. Bejan, Combined 'flow and strength' geometric optimization: internal structure in a vertical insulating wall with air cavities and prescribed strength, *Int. J. Heat Mass Transfer* **45** 3313-3320 (2002).

[10] J. P. D. Hartog, *Strength of Materials, Dover*, New York, 1961.

[11] F. P. Beer, E. R. Johnston, Jr., J. T. DeWolf, *Mechanics of Materials*, 3rd ed., McGraw-Hill, Boston, 2002.

[12] V. S. Arpaci, *Conduction Heat Transfer*, Addison-Wesley, Reading, MA, 1966.

[13] M. Saafi, Effect of fire on FRP reinforced concrete members, *Composite Structures* **58** 11-20 (2002).

[14] L. Gosselin and A. Bejan, Constructal thermal optimization of an electromagnet, *Int. J. Th. Sc.* (Accepted)

[15] R. M. Lawson, Fire engineering design of steel and composite buildings, *J. Const. Steel Res.* **57,** 1233-1247 (2001).